

Dynamic Stability Analysis of Hypersonic Transport During Reentry

Guru Guruswamy*

NASA Ames Research Center, Moffett Field, California 94035

DOI: 10.2514/1.J055018

Dynamic stability analysis is performed for a typical future hypersonic transport vehicle during atmospheric flight. Unsteady aerodynamic data in the form of indicial responses are generated by solving the Navier–Stokes equations. Computations needed at multiple Mach numbers and associated angles of attack are computed in a single job by using dual-level parallel script. Validity of the indicial approach is established by comparing results with experiment and the time-integration method. Flutter boundaries associated with pitch and heave rigid-body degrees of freedom are computed. Effect of position of the mass center on flutter boundaries, which is more predominant in the transonic regime, is shown. This work advances stability analysis procedures for next-generation hypersonic vehicles.

Nomenclature

$[A]$	= aerodynamic matrix
a_h	= location of pitch axis from midlength in b
b	= semilength of the body in feet
C_l, C_m	= sectional lift and moment coefficients
d	= $h/2b$
$\{d\}$	= displacement vector
g	= artificial structural damping coefficient
h	= plunging displacement
$[K]$	= stiffness matrix
k_c, k_b	= reduced frequency, $\omega c/U$ and $\omega b/U$
M	= Mach number
$[M]$	= mass matrix
m	= total mass, slugs
q	= dynamic pressure, $0.5\rho U^2$
Re_L	= Reynolds number based on body length
r_a	= radius of gyration
t	= time, s
U	= speed, ft/s
x_a	= coefficient of mass center location from elastic axis in b
α	= pitching angle, rad
λ	= flutter eigenvalue
μ	= air to mass density ratio, $m/\pi\rho b^2$
ρ	= density of air, slugs/ft ³
$\omega, \omega_f, \omega_h, \omega_\alpha$	= arbitrary, flutter, plunging and pitching frequencies, rad/s
∞	= freestream condition

I. Introduction

FUTURE hypersonic vehicles will include civil transports [1] that will move passengers over long distances in a short period of time. The successful Space Shuttle Orbiter (SSO) design[†] serves as the basis for some of these next-generation concept vehicles. The SSO was dynamically stable because it was rigid compared with

typical transport vehicles. However, to increase the payload capacity, new concept vehicles [2] need larger length-to-width ratios than the SSO configuration. As a result, dynamic stability becomes a more important design consideration for future hypersonic vehicles compared with SSO configurations. The rigid-body modes studied in this paper correspond to the first plunging and pitching modes that determine the primary stability characteristics during reentry [3].

Orbiter flight data were used to perform SSO reentry stability analysis [4]. Because of a lack of advanced computational fluid dynamics (CFD) at the time when SSO was designed, most of the analyses were dependent on linear theories, with corrections based on wind-tunnel data [4]. Based on the pioneering efforts of sponsored by the U.S. Air Force and NASA [5] in using CFD to compute the stability boundaries of two-degree-of-freedom plunge–pitch motions of a typical wing section, several follow-up computations were performed for hypersonic vehicles [6]. Unlike the detailed validation presented in a comparison with linear theory and comparison between time and frequency domain methods [7], most of the later reports have shown ad hoc results [8].

In this paper, flutter boundary computations are made for a typical next-generation hypersonic transport (NGHT) configuration proposed earlier by NASA [9]. The OVERFLOW code [10] for Reynolds-averaged Navier–Stokes (RANS) equations is used to compute the aerodynamic parameters. Grids and time steps are selected based on detailed sensitivity studies similar to that performed by the author in [11,12]. Validation of steady data is made with earlier computations [9]. In this paper, a stability analysis is performed using the unsteady aerodynamic data in the form of indicial responses [13,14]. Ballhaus and Goorjian [14] introduced an approach to generate unsteady aerodynamic data using indicial responses by using a CFD code based on the small perturbation theory. Use of CFD-based indicial responses to compute flutter boundaries was first presented by the author [7]. Recently, the use of indicial responses has been extended to compute unsteady aerodynamic data for a simple unmanned combat aircraft [15], but did not include stability analysis.

In the present paper, the flutter boundary of a typical hypersonic configuration is computed using indicial responses generated by solving the RANS equations. The validity of unsteady aerodynamic data is established by comparing present results using the indicial method with data from experiment and the time-integration method. Stability boundaries are computed using the frequency domain approach, which is more suitable for RANS equations compared with the reduced-order modeling approach, which is mostly applied to Euler equations [16].

Use of RANS simulations in aeroelasticity studies requires large computer resources. This issue is addressed here by using the dual-level parallel protocol called RUNDUA [17], which was recently applied successfully for fast computation of unsteady data for a descending parachute cluster system with a canopy [18].

This paper focuses on solution technology development. The next-generation hypersonic configuration selected for demonstrating the

Presented as Paper 2016-0280 at the AIAA Atmospheric Flight Mechanics Conference, San Diego, CA, 4–8 January 2016; received 12 January 2016; revision received 15 March 2016; accepted for publication 18 March 2016; published online 13 June 2016. This material is declared a work of the U.S. Government and is not subject to copyright protection in the United States. Copies of this paper may be made for personal and internal use, on condition that the copier pay the per-copy fee to the Copyright Clearance Center (CCC). All requests for copying and permission to reprint should be submitted to CCC at www.copyright.com; employ the ISSN 0001-1452 (print) or 1533-385X (online) to initiate your request.

*Senior Scientist, Computational Physics Branch, NASA Advanced Supercomputing Division, Associate Fellow AIAA.

[†]Data available online at http://www.nasa.gov/centers/kennedy/shuttleoperations/orbiters/orbiters_toc.html.

technology does not have structural data. Therefore, structural parameters needed for demonstration are selected from those available in the public domain for similar configurations.

II. Approach

In the present work, the RANS equations [19] are solved numerically using the diagonal form of the Beam–Warming central difference algorithm [20], along with the one-equation Spalart–Allmaras (S–A) turbulence model [21]. The solutions are computed using the OVERFLOW code [10], which uses an overset grid system. The second-order spatial and temporal accuracy options available in the 2.2k version of OVERFLOW are used throughout the present analysis. Dynamic motions are modeled using standard “xml” input files [22].

A. Aeroelastic Equations of Motion

Rigid-body modes play an important role in the stability of NGHT [4]. The stability boundaries corresponding to plunge and pitch modes are of primary importance [4] to develop flight control strategies. In this effort, the structural dynamics of NGHT are first represented by plunging and pitching modes, as shown in Fig. 1. Stability boundaries are computed for freestream conditions starting from $M_\infty = 5.5$ and ending at $M_\infty = 0.50$. Effects of variation in locations of the elastic axis and mass center on stability boundaries are studied.

Because the aeroelastic model is analogous to the two-degree-of-freedom model developed in [7], the following set of equations is used:

$$[\mu k_b^2[M] - [A]] \begin{Bmatrix} \delta \\ \alpha \end{Bmatrix} = \lambda [K] \begin{Bmatrix} \delta \\ \alpha \end{Bmatrix} \quad (1)$$

where $k_b = \text{reduced frequency } \omega b/U$, ω is circular frequency in radians per second, U is speed in feet per second, and b is the semilength of the NGHT; $\delta = h/2b$ and α are displacements corresponding to plunging and pitching motions, respectively. The mass-to-air density ratio is defined as $\mu = m/\pi\rho\alpha^2$, where ρ is the air density and m is the total mass. Structural damping, which is assumed to be small compared with aerodynamic damping, is not included in Eq. (1). However, an artificial damping parameter is included for finding the flutter boundary [23]:

Mass matrix:

$$[M] = \begin{bmatrix} 1 & x_\alpha \\ x_\alpha & \gamma_\alpha^2 \end{bmatrix}$$

Aerodynamic matrix:

$$[A] = \frac{1}{\pi} \begin{bmatrix} 0.5C_{l\delta} & C_{l\alpha} \\ -C_{m\delta} & -2C_{m\alpha} \end{bmatrix}$$

Stiffness matrix:

$$[K] = \frac{1}{\omega_r^2} \begin{bmatrix} \omega_h^2 & 0 \\ 0 & \omega_\alpha^2 r_\alpha^2 \end{bmatrix}$$

where ω_h , ω_α , and ω_r are plunging, pitching, and reference oscillatory frequencies. Radius of gyration r_α is the absolute value of the location of mass center x_α [23].

The eigenvalue λ in Eq. (1) is defined as

$$\lambda = \mu(1 + ig) \left(\frac{b\omega_r}{U} \right)^2$$

where g is the artificial structural damping.

The classical U - g method [23] of finding the flutter boundary is followed. Equation (1) is solved for eigenvalue λ in an iterative process by varying k_b . The aerodynamic matrix $[A]$ for any k_b is computed using the indicial approach [7,13,14]. In the U - g method, flutter point is defined when the artificial damping g changes from positive to negative.

B. Indicial Method

To find the flutter boundary, the aerodynamic matrix $[A]$ of Eq. (1) needs to be computed for various frequencies for a given mode and Mach number. This approach is computationally more efficient than the time-integration method, which will need separate computations for each frequency. Assuming that unsteadiness is caused by a small linear perturbation about a nonlinear steady-state solution, an indicial approach can be used. In the indicial method, only a single computation is required for a given Mach number and mode. The indicial response calculation is carried out by obtaining the flow response to a step change in the given mode of motion. From this response, the solution for all frequencies can be computed by Duhamel’s integration [13]. Figure 2 shows a typical indicial lift response to an arbitrary step change in angle of attack.

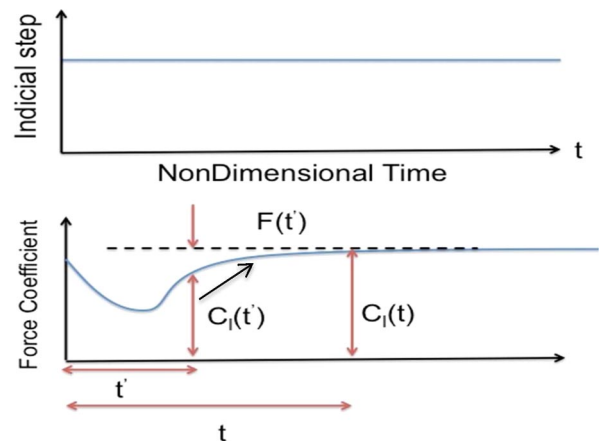


Fig. 2 Typical indicial response.

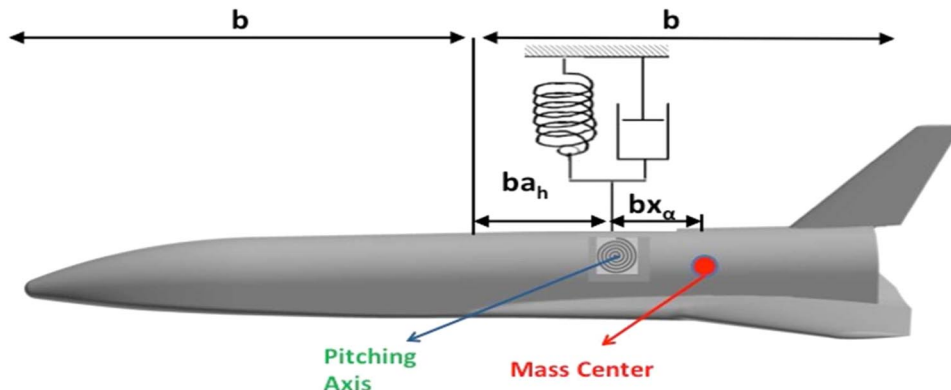


Fig. 1 Two-degree-of-freedom system model of NGHT.

Assuming a sinusoidal motion about a mean angle α_0 with an amplitude of α_1 yields

$$\alpha(t) = \alpha_0 + \alpha_1 e^{i\omega t} \quad (2)$$

Following derivations in [7], real and imaginary parts of the force coefficient can be written as

$$Re[C_{l\alpha}] = C_{l\alpha}(\infty) - \omega \int_0^\infty F(t') \sin(\omega t') dt' \quad (3)$$

$$Im[C_{l\alpha}] = -\omega \int_0^\infty F(t') \cos(\omega t') dt' \quad (4)$$

Similar equations apply for the moment coefficient.

C. Parallel Computing

This effort involves a massive number of cases to compute the large number of conditions to model the descent of NGHT. In [17], a parallel protocol called RUNDUA was developed, which creates an efficient single-job computing environment for multiple cases. If enough processors are used, the resulting wall-clock time for a typical multiple-case calculation series is nearly the same as a single case.

The present approach is aimed toward generating a complete aerodynamic database for stability analysis during descent. The following approach is applied using the OVERFLOW code:

- 1) A set of "Configuration.xml" files that input pitch and plunge motions into OVERFLOW are created.
- 2) Inputs with parameters representing the descent motion (Mach number, angle of attack, Reynolds number) are generated. It is assumed that the number of iterations specified is adequate for convergence for all cases.
- 3) Data are spawned to different directories, which are contiguously numbered.

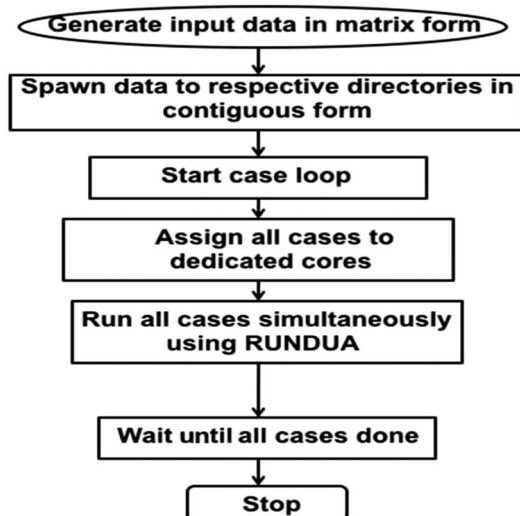


Fig. 3 Flow diagram of RUNDUA [17].

4) All cases are computed, running each case on a different group of cores using "Rank" identification [17].

5) Successful completion of all jobs can be tracked by monitoring the size of the residual files. Once a portable batch system job is successfully completed, all residual files will be the same size. It is assumed that the user has selected appropriate parameters so that results converge at the end of the job completion.

6) After all jobs are successfully completed, force and moment coefficients are extracted from the computed solutions.

Figure 3 shows a flow diagram of RUNDUA.

III. Results

A. Geometry and Grid

The overset surface mesh on the geometry of a NGHT configuration selected from [9] is shown in Fig. 4. Force contributions from the lifting surfaces play a stronger role than other components in stability studies. Given that grid requirements for accurate pressure computations are more stringent for high subsonic Mach numbers than super/hypersonic Mach numbers, grid sensitivity studies are performed for the wing at $M_\infty = 0.90$. A body-fitted near-body (NB) grid with O-H grid topology [12] (wrap around wing section in the x direction and stacked spanwise in the y direction), together with a cap grid for the wing tip, is used to model the vehicle. We start with a fine grid with 816 chordwise points and 25 spanwise stations generated using the OVERGRID grid tool [24]. Based on earlier grid sensitivity studies [12], a normal spacing of $0.000025c$ (c is the root chord length of the wing) with a surface-stretching factor of 1.125 is used. This yields a y^+ value (one grid point away from the surface) that varies between 0.959 and 1.14, which is adequate to resolve boundary-layer flows at the surface. The y^+ value is a nondimensional distance used to describe the fineness of a mesh for a particular flow pattern. It is important in turbulence modeling to determine the proper size of the grid cells near domain walls. The turbulence model wall laws have restrictions on the y^+ value at the wall. The standard S-A model [21] requires a wall y^+ value about one. A faster flow near the wall will produce higher values of y^+ , and so the grid size near the wall must be reduced.

Figure 5 shows the effect of the size of the x grid on the lift coefficient (Coef). Starting from the selected fine grid of size 816 points, coarser grids are generated by removing alternate grid points starting from the second point. In Fig. 5, it is observed that about 409

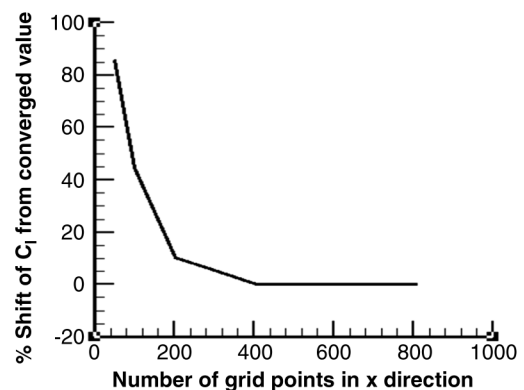


Fig. 5 Effect of chordwise grid points.

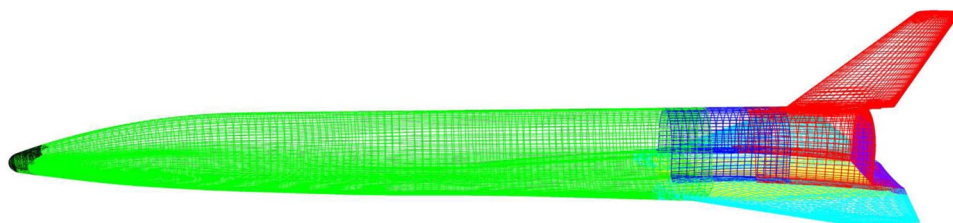


Fig. 4 Surface grids.

points are adequate. Based on the plot of lift coefficient vs the number span stations in Fig. 6, about 30 spanwise stations are adequate.

The rest of the NB grids are selected from those used in [9]. Next, the off-body (OB) grids are determined based on the grid refinement studies. Adequacy of the OB grid depends on the spacing of level 1 (closest to NB grids) grids. Figure 7 shows that a level 1 grid spacing of 0.25% of the length of the vehicle is adequate. Figure 8 shows that the outer boundary location of OB grid at about four lengths of the vehicle is adequate. Based on these grid sensitivity studies, a total of 20 million points for near-body grids and 25 million points for off-body grids are required.

B. Steady-State Computations

Computations are made for 100 cases with decreasing Mach number from 5.5 to 0.5 in decrements of 0.05 and corresponding

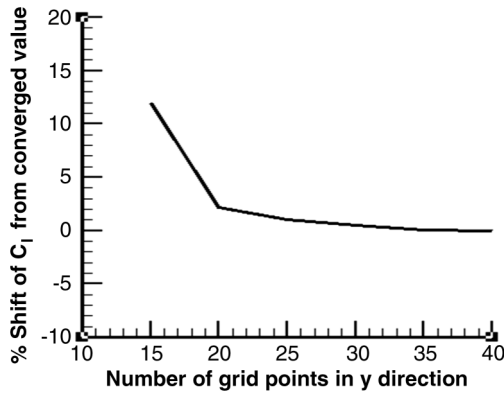


Fig. 6 Effect of spanwise grid points.

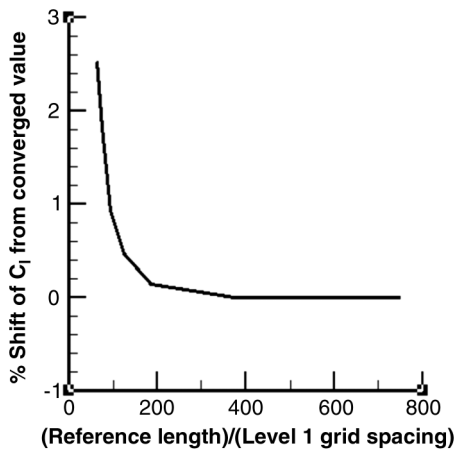


Fig. 7 Sensitivity of OB grid spacing.

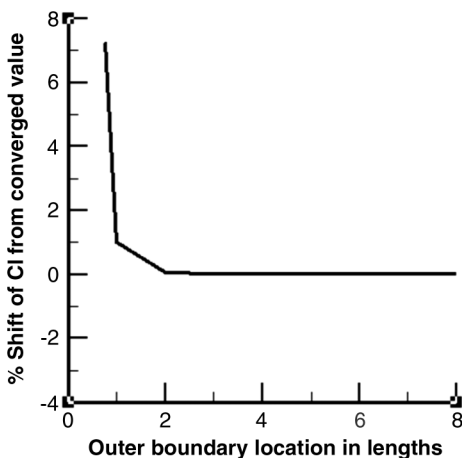


Fig. 8 Sensitivity of outer boundary location.

angle of attack α decreasing from 12 to 2 deg in decrements of 0.1. The Reynolds number based on length increases from 10 to 100 million. It is assumed that this event takes place in the last 30 s of flight before touchdown. Based on the residual convergence shown in Fig. 9 and lift convergence in Fig. 10 for $M_\infty = 0.90$, 40,000 iterations were adequate for steady-state computations.

Figure 11 shows the comparison of C_p with earlier results from the Langley Research Center (LaRC) using the original grid (106 chordwise points) [9]. The present fine (409) and finer (816) grids show almost the same C_p distribution. Compared with the original grid, both fine and finer grids show changes in the upper surface C_p up to about 25% chord and near the shock wave. This comparison supports numerical verification requirements of further results presented in the paper. Figure 12 shows the plots of Mach number,

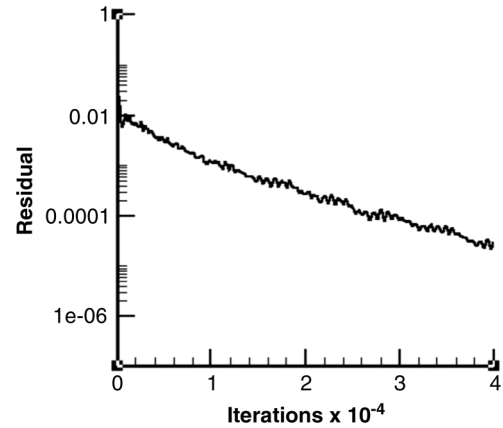


Fig. 9 Residual convergence.

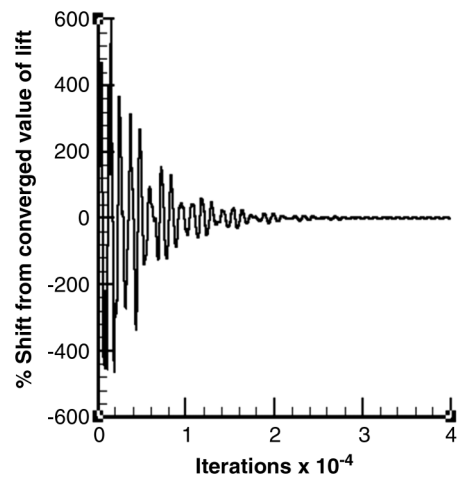


Fig. 10 Lift convergence.

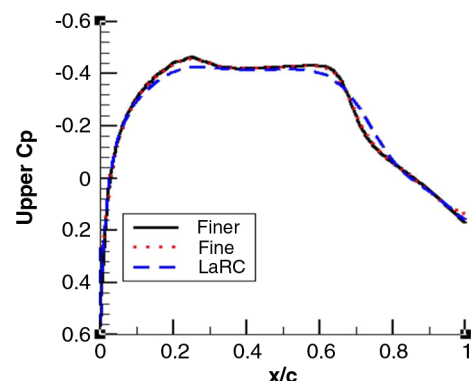
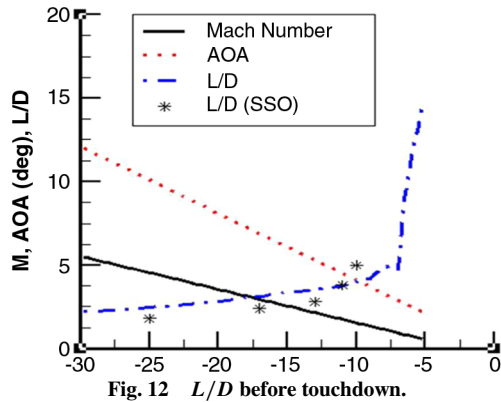
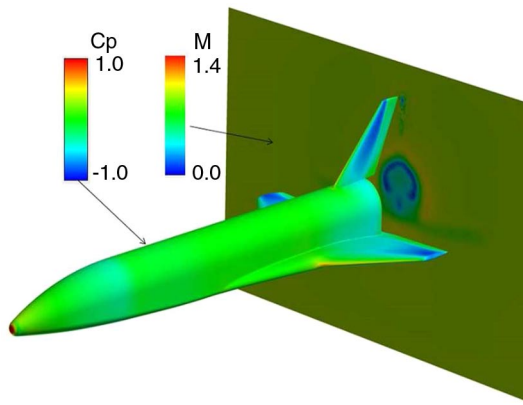
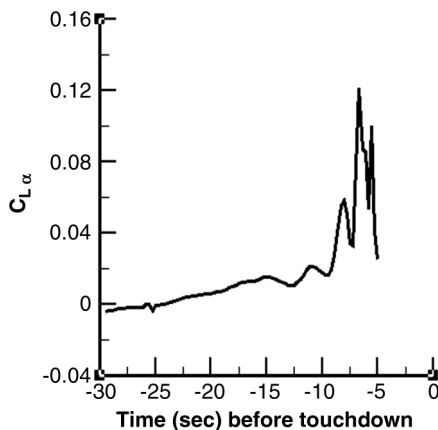


Fig. 11 C_p at $M_\infty = 0.5$, $\alpha = 0.0$ deg.

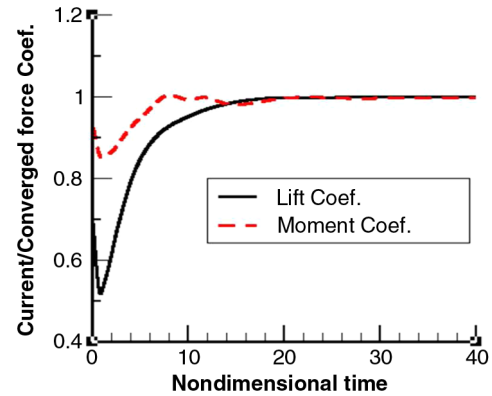
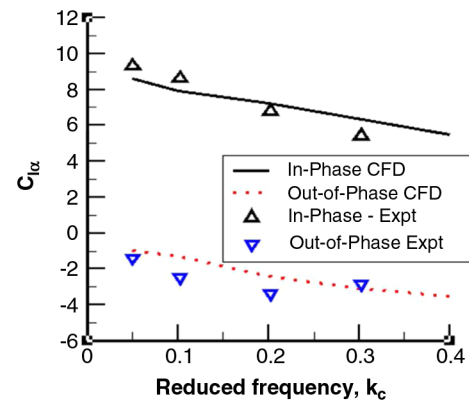
Fig. 12 L/D before touchdown.Fig. 13 C_p and Mach contours at $M_\infty = 0.90$.Fig. 14 Rate of change in lift with respect to α .

angle of attack (AOA), and lift/drag L/D with respect to time before touchdown, along with results for the SSO. The Reynolds number based on body length Re_L is assumed to linearly increase from 10 to 100 million. L/D rapidly increases as the speed climbs to around transonic Mach numbers. Computed results for the geometry are qualitatively comparable to those reported for the SSO [3]. Figure 13 shows surface C_p and Mach contours downstream during descent. Figure 14 shows the static stability derivative, the rate of lift with angle of attack as a function of time to touchdown.

IV. Dynamic Stability Analysis

A. Validation

To compute stability boundaries, unsteady data are generated using the indicial method [7]. The validity of generating indicial data using OVERFLOW is verified by comparing the results with

Fig. 15 Indicial responses of sectional lift and moments for the NACA 64A10 airfoil at $M_\infty = 0.80$.Fig. 16 Validation of indicial results with the experiment (Expt) for the NACA 64A10 airfoil at $M_\infty = 0.80$.

experimental data for an oscillating NACA 64010 airfoil [25]. The airfoil was modeled using a single grid with 201 chordwise and 75 normal directional grid points, which was found adequate for accuracy based on sensitivity studies. The indicial response was computed at $M_\infty = 0.8$ using a step angle of attack of 1.0 deg, which is in the linear perturbation range of the nonlinear steady-state solution with a moderate shock wave. As shown in Fig. 15, the computation required 6000 time steps (or nondimensional time 40) for the response to reach a constant value. Figure 16 shows good comparison of in-phase and out-of-phase values of $C_{L\alpha}$ for increasing reduced frequencies $k_c = \omega c/U$, where c is the chord length. As expected, the OVERFLOW code, which is based on the previously demonstrated Beam-Warming algorithm for indicial response computations [26], is valid for further indicial responses in this paper.

B. Demonstration for Next-Generation Hypersonic Transport

The final grid of 20 million near-body grids points, decided based on grid sensitivity studies, is used for the rest of the unsteady computations. The time step is established based on the temporal studies.

It is found that 3600 steps per cycle (NSPC) with 15 Newton subiterations (NWIT) are adequate for accurate unsteady responses for $k_b = 1.13$ (corresponding to assumed values of $M_\infty = 3.0$, oscillating frequency 4 Hz, and $b = 130$ ft [2]). The corresponding nondimensional time step size is 0.00232.

Table 1 shows a comparison between stability derivatives of pitching motion obtained by indicial and time-integration approaches at representative $M_\infty = 0.90$ for a typical section of the wing's 50% semispan. Time-integration required three cycles with NSPC = 3600 for each frequency, whereas 3000 steps were required for the indicial response with a 0.5 deg step to converge. Wall-clock time needed for indicial computation is one-eighteenth of the time required by the time-integration approach. The flutter speed

Table 1 $C_{l\alpha}$ for section of the wing at 50% semispan

Parameter	Value				
Reduced frequency k_c	0.1	0.2	0.3	0.4	0.5
Indicial: in phase	8.4408	88.001	7.557	6.891	6.127
Time integration: in phase	8.051	7.712	7.237	6.567	5.978
Indicial: out of phase	-1.338	-1.701	-2.025	-2.401	-3.001
Time integration: out of phase	-1.233	-1.654	-1.934	-2.350	-2.905

computed by using Eq. (1) differed by only about 5% between the two approaches. The rest of the computations will be performed for the full configuration using the indicial method.

Flutter boundary computations for the full configuration are made for 100 cases in the last 30 s of descent, during which Mach number decreases from 5.5 to 0.5 in decrements of 0.05, and the corresponding angle of attack α decreases from 12 to 2 deg in decrements of 0.1. The Reynolds number based on length increases from 10 million to 100 million. From numerical experiments, it is found that 6000 steps with $NWIT = 15$ are adequate for all cases for indicial responses to converge with 0.5 deg step pitching at two-thirds length (as suggested in [27]). All cases were completed in 17.5 wall-clock hours using 4000 cores with 40 cores per case.

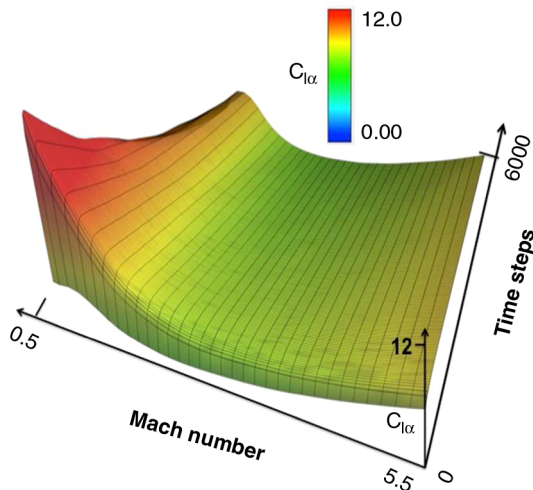


Fig. 17 Indicial responses of $C_{l\alpha}$ for a full configuration.

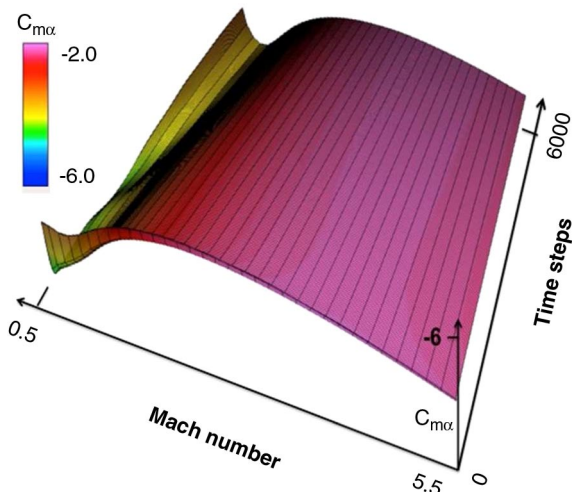


Fig. 18 Indicial responses of the $C_{m\alpha}$ configuration.

Figures 17 and 18 show carpet plots of indicial time responses in time for $C_{l\alpha}$ and $C_{m\alpha}$, respectively. We find that dynamic responses are more sensitive near transonic Mach numbers compared with the response at higher Mach numbers.

Flutter boundary computations were made by solving Eq. (1). Based on the gross weight 4080 lbf and length of 62.5 ft given in [27] (Table 1 and Fig. 3) the value of $\mu = 184$ at 60,000 ft altitude. The typical values of elastic axis location $a_h = 0.33b$ and $\omega_h/\omega_\alpha = 0.25$ [6] are assumed. Computations are made for the mass center in front of the elastic axis at $x_\alpha = -0.05, -0.1, \text{ and } -0.15$; γ_α is absolute value x_α . Figures 19 and 20 show flutter speed and corresponding frequency with respect to time before landing. Flutter speed, which gradually decreases in time, takes a dip around transonic Mach numbers, a phenomenon similar to that observed for advanced transport aircraft [28,29]. Also, a variation in x_α has effects mostly near the transonic regime, showing that the vehicle is less stable when the mass center is closer to the pitching axis. Flutter frequency is almost constant until the transonic regime.

Following the discussions for two-dimensional airfoils in [7,29], the dip in Fig. 19 can be explained as follows. For $x_\alpha = -0.1$, Figs. 21 and 22 show a plot of a real part of $C_{l\alpha}$ and the corresponding location of the center of pressure x_{cp} measured from midbody in semilength b , respectively. As the Mach number decreases, $C_{l\alpha}$ decreases until the transonic regime and then starts rising rapidly. An increase in $C_{l\alpha}$ corresponds to a reduction in flutter speed [30], as seen in Fig. 19. During the transonic regime, x_{cp} moves toward the mass center and starts stabilizing the system. As a result, the flutter speed starts increasing after the transonic regime. After reaching the dip, flutter speed starts increasing corresponding to drop in $C_{l\alpha}$.

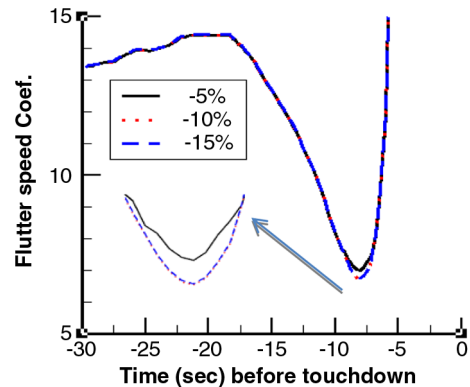


Fig. 19 Flutter boundary during descent of NGHT for $x_\alpha = 0.05, -0.1, \text{ and } -0.15$.

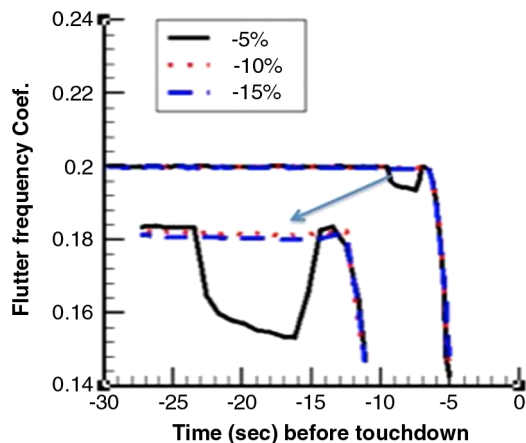


Fig. 20 Flutter frequencies during descent of NGHT $x_\alpha = 0.05, -0.1, \text{ and } -0.15$.

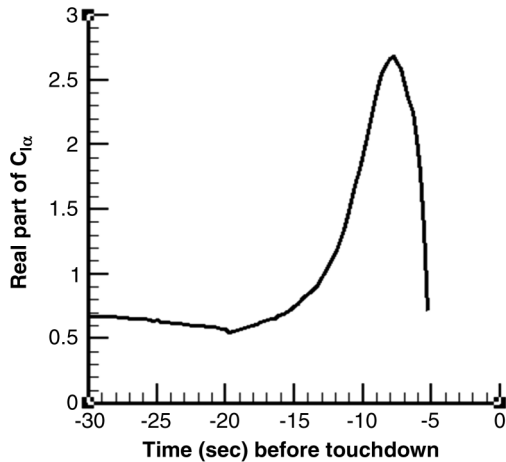


Fig. 21 Change in real part of C_{la} with time.

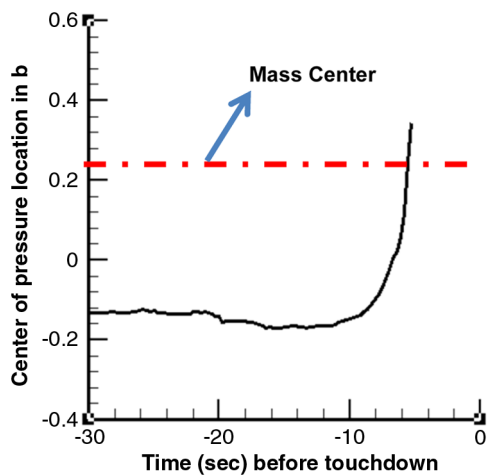


Fig. 22 Change in center of pressure location with time.

V. Conclusions

An advanced technology is developed, validated, and demonstrated for cost-effectively computing the onset of instability for future hypersonic transport. A computational procedure based on the Navier–Stokes equations is presented to compute the possible onset of instability associated with small perturbations for future hypersonic transport during reentry. Static stability derivatives compare qualitatively well with a similar configuration. The indicial approach is found to be a cost-effective approach to predict the onset of dynamic instability associated with flutter. For small perturbations, results from the indicial response approach compare well with unsteady experiments of an oscillating airfoil and computed results using the time-integration method. Computations on a typical section show that the indicial method requires one-eighteenth the wall-clock time of the time-integration method. Dual-level parallel protocols facilitated the generation of large unsteady aerodynamic data for a complete descent in practical time. With the use of 4000 cores, static stability derivatives for 100 cases with varying Mach numbers and angles of attack are computed in 2.5 h of wall-clock time, just 7% more than the wall-clock time required to run a single case in a single job using other procedures. Dynamic indicial responses for all 100 cases needed 17.5 h of wall-clock time. The present study shows that the critical period during descent is in the transonic regime. For the assumed parameters of a typical transport configuration, the flutter boundary shows a dip around the transonic regime. In addition, the location of the mass center with respect to the pitching axis is more sensitive near the transonic Mach number regime than at other Mach numbers. This work, based on the state-of-the-art high-fidelity analysis procedure, will benefit the design of future hypersonic transport vehicles.

Acknowledgments

The author thanks Pieter Buning of NASA Langley Research Center for providing consultations regarding the OVERFLOW code. This work is performed under the supercomputing technology demonstration activities of the NASA Advanced Supercomputing Division at NASA Ames Research Center.

References

- [1] Sippel, M., "Promising Roadmap Alternatives for the SpaceLiner," *ACTA Astronautica*, Vol. 66, Nos. 11–12, June–July 2010, pp. 1652–1658.
doi:10.1016/j.actaastro.2010.01.020
- [2] Eggers, T., Dittrich, R., and Vrvill, R., "Numerical Analysis of the SKYLON Space Plane in Hypersonic Flow," *17th AIAA International Space Planes and Hypersonic Systems and Technologies Conference*, AIAA Paper 2011-2298, April 2011.
- [3] Chyu, W. J., Cavin, R. K., and Erickson, L. L., "Static and Dynamic Stability Analysis of the Space Shuttle Vehicle-Orbiter," NASA TP 1179, March 1978.
- [4] Iliff, K. W., and Shaper, M. F., "Extraction of Stability and Control Derivatives from Orbiter Flight Data," NASA TM 4550, June 1993.
- [5] Yang, T. Y., Guruswamy, G. P., Striz, A. G., and Olsen, J. J., "Flutter Analysis of a NACA 64A006 Airfoil in Small Disturbance Transonic Flow," *Journal of Aircraft*, Vol. 17, No. 4, April 1980, pp. 225–232.
doi:10.2514/3.44652
- [6] McNamara, J. J., and Friedmann, P. P., "Aeroelastic and Aerothermoelastic Analysis in Hypersonic Flow: Past, Present, and Future," *AIAA Journal*, Vol. 49, No. 6, 2011, pp. 1089–1122.
doi:10.2514/1.J050882
- [7] Guruswamy, G. P., "Aeroelastic Stability and Time Response Analysis of Conventional and Supercritical Airfoils in Transonic Flow by the Time Integration Method," Ph.D. Thesis, Purdue Univ., West Lafayette, IN, Dec. 1980, <http://docs.lib.purdue.edu/dissertations/AAI8113693/>.
- [8] McNamara, J. J., Friedmann, P. P., Powell, K. G., Thuruthimattam, B. J., and Bartels, R. E., "Aeroelastic and Aerothermoelastic Behavior in Hypersonic Flow," *AIAA Journal*, Vol. 46, No. 10, Oct. 2008, pp. 2531–2610.
doi:10.2514/1.36711
- [9] Murphy, K. J., Buning, P., Bandu, N. P., Scallion, W. I., and Jones, K. M., "Overview of Transonic to Hypersonic Stage Separation Tool Development for Multi-Stage-to-Orbit Concepts," AIAA Paper 2004-2595, Jan. 2004.
- [10] Nichols, R. H., Tramel, R. W., and Buning, P. G., "Solver and Turbulence Model Upgrades to OVERFLOW2 for Unsteady and High-Speed Applications," *36th AIAA Fluid Dynamics Conference*, AIAA Paper 2006-2824, June 2006.
- [11] Guruswamy, G. P., "Navier–Stokes–Equations–Based Computations of Launch Vehicles Experiencing Forced Coupled Oscillations," *Journal of Spacecraft and Rockets*, Vol. 52, No. 1, 2015, pp. 299–302.
- [12] Guruswamy, G. P., "A Modular Approach to Model Oscillating Control Surface Using Navier–Stokes Equations," *Fifth Decennial AHS Aeromechanics Specialists' Conference*, Jan. 2014, <https://vtol.org/store/product/a-modular-approach-to-model-oscillating-control-surfaces-using-navierstokes-equations-9313.cfm>.
- [13] Tobak, M., and Pearson, W. E., "A Study of Nonlinear Longitudinal Dynamic Stability," NASA TR-209, 1964.
- [14] Ballhaus, W. F., and Goorjian, P. M., "Computation of Unsteady Transonic Flows by the Indicia Method," *AIAA Journal*, Vol. 16, No. 2, Feb. 1978, pp. 117–124.
- [15] Ghoreyshi, M., and Cummings, R. M., "Aerodynamics Modeling of a Maneuvering Aircraft Using Indicial Functions," *50th AIAA Aerospace Sciences Meeting*, AIAA Paper 2012-0689, Jan. 2012.
- [16] Guruswamy, G. P., "Frequency Domain Flutter Boundary Computations Using Navier–Stokes Equations on Superclusters," *Journal of Aircraft*, Vol. 51, No. 5, Sept.–Oct. 2014, pp. 1640–1642.
- [17] Guruswamy, G. P., "Dual Level Parallel Computations for Large Scale High-Fidelity Database to Design Aerospace Vehicles," NASA/TM 2013-216602, Sept. 2013.
- [18] Guruswamy, G. P., "Fast Database Generation for Parachute Cluster Design Using Navier–Stokes Equations on Supercomputers," *23rd AIAA Aerodynamic Decelerator Systems Technology Conference*, AIAA Paper 2015-2170, April 2015.
- [19] Peyret, R., and Viviand, H., "Computation of Viscous Compressible Flows Based on Navier–Stokes Equations," AGARD AG-212, 1975.
- [20] Beam, R. M., and Warming, R. F., "An Implicit Factored Scheme for the Compressible Navier–Stokes Equations," *AIAA Journal*, Vol. 16, No. 4, 1978, pp. 393–402.

- [21] Spalart, P. R., "Direct Simulation of a Turbulent Boundary Layer," *Journal of Fluid Mechanics*, Vol. 187, Feb. 1988, pp. 61–98.
- [22] Murman, S. M., Chan, W. M., Aftosmis, M. J., and Meakin, R. L., "An Interface for Specifying Rigid-Body Motion for CFD Applications," AIAA Paper 2003-1237, Jan. 2003.
- [23] Fung, Y. C., *Introduction to the Theory of Aeroelasticity*, Dover, New York, 1968, pp. 211–242.
- [24] Chan, W. M., "Developments in Strategies and Software Tools for Overset Structured Grid Generation and Connectivity," AIAA Paper 2011-3051, June 2011.
- [25] Davis, S. S., and Malcolm, G. N., "Experimental Unsteady Aerodynamics of Conventional and Supercritical Airfoils," NASA TM 81221, Aug. 1980.
- [26] Guruswamy, G. P., and Tu, E. L., "Navier–Stokes Computations on Flexible Advanced Transport-Type Wing Configurations in Transonic Regime," AIAA Paper 1994-1725, April 1994.
- [27] Pamadi, B. N., Covell, P. F., Tartabini, P. V., and Murphy, K. J., "Aerodynamic Characteristics of Glide Back Performance of Langley Glide Back Booster," *22nd Applied Aerodynamics Conference*, AIAA Paper 2004-5382, Aug. 2004.
- [28] Farmer, M. G., and Hanson, P. W., "Comparison of Super-Critical and Conventional Wing Flutter Characteristics," NASA TM-X-72837, 1976.
- [29] Yang, T. Y., Guruswamy, G. P., Striz, A. G., and Olsen, J. J., "Reply by Authors to H.P.Y. Hitch," *Journal of Aircraft*, Vol. 18, No. 2, Feb. 1981, pp. 159–160.
- [30] Bisplinghoff, R. L., and Ashley, H., *Principals of Aeroelasticity*, Dover, New York, 1962, pp. 280–402.

R. K. Kapania
Associate Editor